J. Marine Sci. Appl. (2017) 16: 208-215
DOI: 10.1007/s11804-017-1404-z

Helical Wire Stress Analysis of Unbonded Flexible Riser Under Irregular Response

Kunpeng Wang* **and Chunyan Ji**

School of Naval Architecture and Ocean Engineering, Jiangsu University of Science and Technology, Zhenjiang 212003, China

Abstract: A helical wire is a critical component of an unbonded flexible riser prone to fatigue failure. The helical wire has been the focus of much research work in recent years because of the complex multilayer construction of the flexible riser. The present study establishes an analytical model for the axisymmetric and bending analyses of an unbonded flexible riser. The interlayer contact under axisymmetric loads in this model is modeled by setting radial dummy springs between adjacent layers. The contact pressure is constant during the bending response and applied to determine the slipping friction force per unit helical wire. The model tracks the axial stress around the angular position at each time step to calculate the axial force gradient, then compares the axial force gradient with the slipping friction force to judge the helical wire slipping region, which would be applied to determine the bending stiffness for the next time step. The proposed model is verified against the experimental data in the literature. The bending moment–curvature relationship under irregular response is also qualitatively discussed. The stress at the critical point of the helical wire is investigated based on the model by considering the local flexure. The results indicate that the present model can well simulate the bending stiffness variation during irregular response, which has significant effect on the stress of helical wire.
Keywords: unbonded flexible riser, interlayer interaction, helical wire stress, local flexure, bending stiffness variation, irregular response

Article ID: 1671-9433(2017)02-0208-08

1 Introduction

The flexible riser is a key component of an oil and gas production system comprising polymeric and metallic layers with different functions. Polymeric layers often provide sealing or insulation for internal and external fluids and reduce metallic friction. Metallic layers generally include the innermost carcass, profiled Z-shaped pressure armor layer, and tensile armor layer. The first two kinds of layers are interlocked and wound at a lay angle close to 90° and mainly resist the inward and outward pressures, respectively. The tensile armor layers with rectangular cross-section helical wires have two or four layers, and are cross-wound at lay angles between 20° and 55° (De Sousa *et al*., 2012). This kind of layer is designed to carry the tension, torque, and pressure end cap effect.

Compared with the conventional steel riser, the flexible riser can withstand large bending deformation without compromising the axial stiffness and the pressure integrity. It also has advantages in the aspects of storage in long lengths on the reel and in the installation cost (de Sousa *et al*., 2009). However, its complex construction significantly increases the difficulty of performance assessment, thereby attracting much research attention. A helical wire is one of the critical components prone to fatigue failure. An integrated model for the flexible riser should first be established to predict the fatigue damage of the helical wire. The commonly used method is analytical formulation, which can partly explain the nonlinear mechanism of flexible pipes and is time efficient (Wang and Chen, 2011). Witz and Tan (1992a; 1992b) proposed an analytical model to predict the axial–torsional and bending structural behaviors of a flexible pipe. Kraincanic and Kebadze (2001) investigated the slip initiation and progression in the helical wire of a flexible pipe and derived the bending moment–curvature relationship, which showed good agreement with the experimental data. Bahtui *et al*. (2009) proposed an approach to model the axisymmetric and bending response in a whole matrix and compared it with a detailed FE model.

The helical wire stress can be further investigated based on analytical formulations. Leroy and Estrier (2001) studied the dynamic stress in the helical wire based on its geometrical, friction, and equilibrium equations. They then validated the proposed method using the measured strain. Sævik (2011) applied two alternative approaches to predict the bending stress in the helical wire of a flexible pipe, in which the nonlinear bending moment–curvature relationship and the sandwich beam theory were used to describe the stick–slip behavior of the helical wire. The obtained stress is compared with the experimental data, and the results showed good agreement. Skeie *et al*. (2012) investigated the helical wire stress considering the local bending, and demonstrated the stress range at different circumferential positions. Tang *et al*. (2015) studied the validity and limitation of several analytical models for the bending stress calculation of the helical wire by using a detailed FE model.

Received date: 29-Nov-2016
Accepted date: 07-Mar-2017
Foundation item: Supported by the Natural Science Foundation of Jiangsu Province under Grant No. BK20160557, and the General Program for Colleges and Universities in Jiangsu Province under Grant No. 16KJD570001
***Corresponding author Email:** wangkunpeng@just.edu.cn

The traditional method for fatigue damage assessment often first performs a global analysis of the flexible riser using constant bending stiffness and then transports the global response to the local model for the stress calculation of the helical wire (de Sousa *et al*., 2012). Tan *et al*. (2007) implemented the in-house hysteretic model of Wellstream as an external function of OrcaFlex to simulate the global response of the flexible riser. The results illustrated the necessity of considering the bending stiffness variation in the global analysis. Although researches on the flexible riser have been extensively conducted in the recent years, the stress characteristics of the helical wire under an irregular response, including the bending stiffness variation, is still not investigated and presented.

This study presents a feasible model of the flexible riser under an irregular response and investigates the stress of the helical wire considering local flexure. The interlayer interaction under axisymmetric loads in the model is simulated by setting up dummy springs. The interlayer pressures are then obtained for the bending analysis. The bending stiffness is updated at each time step during the response analysis by determining the slipping region of the helical wires. An eight-layer flexible pipe in Witz (1996) is employed to verify the model. The stress at the critical point of the helical wire considering local flexure is then investigated.

2 Methodology

The flexible riser has several different kinds of layers (Fig. 1), which are often treated individually, but have the same axial displacement u_z, axial rotation ϕ_z, rotation ϕ_x about x axis, and ϕ_y about y-axis (Fig. 2). The radial displacement u_r of each layer is modeled individually because the separation of the adjacent layers is allowed.

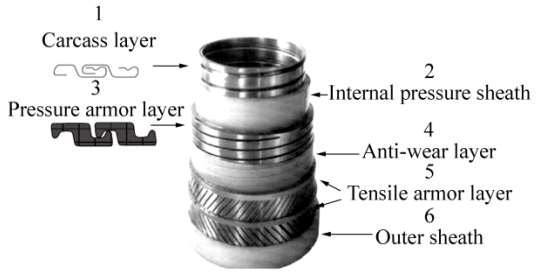

Fig. 1 Typical flexible riser components (De Sousa *et al*., 2014)

The following assumptions are applied in the present study to formulate the flexible riser:

1) The helical wire only slides along its axial direction (i.e., the loxodromic curve) (Sævik, 2011).

2) The curvature is constant along the flexible riser element.

3) The interlayer contact pressure results from an axisymmetric response and remains constant during the bending behavior.

4) The sliding friction of the helical wire is equal to the maximum static friction.

5) The initial state of the helical wire is approximately a stress-free state (Skeie *et al*., 2012).

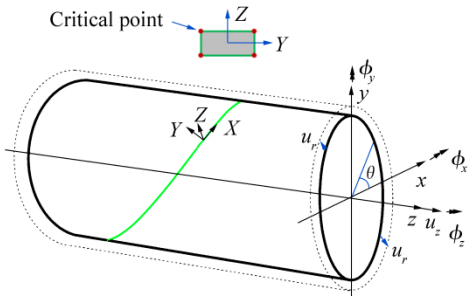

Fig. 2 Displacement symbols of a layer and the critical point of helical wire

2.1 Axisymmetric formulation

The axisymmetric loads include the axial tension, torque, and internal and external pressures. The related tangent stiffness should be obtained to solve the displacements under these loads. The carcass armor and the pressure armor layer are often equivalent to the orthotropic cylinder. de Sousa *et al*. (2009, 2014) proposed an effective equivalent method based on the analogy between the helical tendon and the orthotropic shell. The method would not be detailed in the present study for brevity. After equivalence, the flexible riser layers can be divided into the cylindrical and helical layer categories. The helical layer mainly includes the tensile armor layer and the anti-wear layer.

The stress–strain relationship of a cylinder can be expressed as follows based on the Hooke's law:

$$\begin{Bmatrix}\sigma_1\\ \sigma_2\\ \sigma_{12}\end{Bmatrix}=\begin{bmatrix}\frac{E_1}{1-\nu_{12}\nu_{21}} & \frac{\nu_{12}E_1}{1-\nu_{12}\nu_{21}} & 0\\ \frac{\nu_{21}E_2}{1-\nu_{12}\nu_{21}} & \frac{E_2}{1-\nu_{12}\nu_{21}} & 0\\ 0 & 0 & G_{12}\end{bmatrix}\begin{Bmatrix}\varepsilon_1\\ \varepsilon_2\\ \gamma_{12}\end{Bmatrix} \quad (1)$$

where E, v, and G are the Young's modulus, Poisson ratio, and shear modulus, respectively. Subscripts 1 and 2 represent the axial and circumferential directions, respectively. For the isotropic polymeric layer, E_1 is equal to E_2 and ν_{12} is equal to ν_{21}. The strains, as a function of the axisymmetric displacements, are described by the following equations (McNamara and Harte, 1989):

$$\varepsilon_1=\frac{u_z}{L},\ \varepsilon_2=\frac{u_r}{R},\ \gamma_{12}=R\frac{\phi_z}{L} \quad (2)$$

where L and R represent the length and the radius of the cylinder, respectively.

The linearized axial strain for the helical layer is expressed as follows (Sævik, 2011):

$$\varepsilon_{0X}=\frac{u_z}{L}\cos^2(\alpha)+\frac{u_r}{R}\sin^2(\alpha)+R\frac{\phi_z}{L}\sin(\alpha)\cos(\alpha) \quad (3)$$

where α is the lay angle of the helical wire.

The treatment of the interlayer interaction should be elaborated under the axisymmetric loads. Witz and Tan

(1992a) and Bahtui *et al*. (2009) investigated the modeling of the interlayer interaction based on the structural continuity and equilibrium along the radial direction. The former described the pressure difference of the helical wire as a function of the local curvature, bending moment, and torque, whereas the latter referred to the research work of Lanteigne (1985), where the pressure difference of the helical wire was related with the axial strain. The interlayer interaction in the present study is simulated by setting dummy springs between the medium lines of the adjacent layers (Fig. 3).

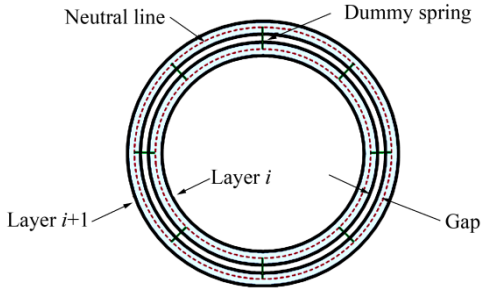

Fig. 3 Sketch of the interlayer interaction model

The strain energy U and the work W related with the external force are obtained as follows based on the principle of virtual work:

$$U=\sum_{i=1}^{N}\iiint\left(\frac{1}{2}\boldsymbol{\sigma}_i^{\mathrm{T}}\boldsymbol{\varepsilon}_i\right)\mathrm{d}V+\sum_{i=1}^{N-1}\frac{1}{2}Lk_i\left(u_{r,i}-u_{r,i+1}\right)^2 \tag{4}$$

$$W=Fu_z+T\phi_z+\left[P_{\mathrm{in}}R_2^2\left(\frac{u_z}{L}+\frac{2u_{r,2}}{R}\right)-P_{\mathrm{out}}R_N^2\left(\frac{u_z}{L}+\frac{2u_{r,N}}{R}\right)\right]\pi L \tag{5}$$

where N is the number of layers; subscript i is the ith layer; F and T are the axial force and torque, respectively; and P_{in} and P_{out} are the internal and external pressures, respectively. The internal pressure is directly exerted on the internal pressure sheath, considering that the innermost carcass armor is not waterproof. k is the stiffness of the dummy springs, which would be iteratively adjusted based on the interlayer penetration and the separation condition. The interlayer penetration corresponds to an increasing k_i, whereas the interlayer separation corresponds to a decreasing k_i. The interlayer contact pressure can be calculated based on the convergent k_i and the interlayer radial displacement.

The equilibrium equation of the flexible riser in the form of a matrix can be given as follows by letting $U = W$:

$$\begin{bmatrix} K_{11} & K_{12} & \cdots & K_{1j} & \cdots \\ K_{21} & K_{22} & \cdots & K_{2j} & \cdots \\ \vdots & \vdots & \ddots & 0 & 0 \\ K_{j1} & K_{j2} & 0 & K_{jj} & K_{j(j+1)} \\ \vdots & \vdots & 0 & K_{(j+1)j} & \ddots \end{bmatrix}\begin{Bmatrix} \frac{u_z}{L} \\ \frac{\phi_z}{L} \\ \vdots \\ \frac{u_{r,j-2}}{R_{j-2}} \\ \vdots \end{Bmatrix}=\begin{Bmatrix} \overline{F} \\ T \\ \vdots \\ \overline{P}_{j-2} \\ \vdots \end{Bmatrix} \tag{6}$$

where the matrix dimension is $(N+2)\times(N+2)$ and the elements are given in the Appendix.

2.2 Axisymmetric formulation

The bending nonlinearity of the flexible riser is mainly related with the stick–slip behavior of the helical wire. The helical wire starts to slip at the position near the neutral surface when the bending curvature reaches the minimum critical value, and then propagates with the increasing curvature until full slippage happens. The non-slipping and slipping axial strains induced by the bending response are presented as follows (Dong *et al*., 2013):

$$\varepsilon_{0X}=\begin{cases} R\cos^2(\alpha)\sin(\theta)\kappa & \text{Sticking} \\ \left(P_1f_1+P_2f_2\right)\dfrac{R\theta}{E\sin(\alpha)t} & \text{Slipping} \end{cases} \tag{7}$$

where κ is the curvature; θ is the angular position in the range of [0, π/2] (Fig. 2); P_1 and P_2 are the internal and external pressures of the helical armor obtained based on the above axisymmetric model; f_1 and f_2 are the corresponding friction coefficients; and t is the layer thickness. This study takes the bending around the x axis as an example. Thus, κ is equal to ϕ_x/L.

The equilibrium between the strain energy and the work done by the bending moment under the virtual curvature increment can be expressed as follows because the slipping part of the helical wire keeps stress constant and would not contribute to the strain energy associated with the curvature variation:

$$\Delta M_x\delta\phi_x=\iiint_V E\left(\delta\varepsilon_{0X}\right)^2\mathrm{d}v=\int_0^L\int_{R-t/2}^{R+t/2}\left[4\int_{\theta_{cr}}^{\pi/2}ER^2\cos^4(\alpha)\sin^2(\theta)\left(\frac{nb}{2\pi}\mathrm{d}\theta\right)\right]\mathrm{d}r \tag{8}$$

$$\frac{\mathrm{d}l}{\cos\alpha}\left(\frac{\delta\phi_x}{L}\right)^2=EI_0\left(1-\frac{2}{\pi}\theta_{cr}+\frac{1}{\pi}\sin(2\theta_{cr})\right)\frac{\delta\phi_x}{L}\delta\phi_x$$

Thus, the tangent bending stiffness of the helical armor is given as:

$$EI=EI_0\left(1-\frac{2}{\pi}\theta_{cr}+\frac{1}{\pi}\sin(2\theta_{cr})\right) \tag{9}$$

where ΔM_x is the bending moment around the x axis associated with the virtual curvature increment of $\delta\kappa=\delta\phi_x/L$; θ_{cr} is the boundary of the sticking and slipping parts in the range of [0, π/2]; and $EI_0=nEAR^2\cos^3(\alpha)/2$ is the non-slipping bending stiffness.

Conventional studies often investigate the full loop of the hysteretic bending moment–curvature relationship, which only provides the bending stiffness under a regular response. The present study tracks the axial stresses along angular positions at each time step to determine the slipping region (i.e., θ_{cr}). The bending stiffness is then calculated for the next time step. The slipping region can be determined as follows based on the axial stress gradient (Tan *et al*., 2007, Dong *et al*., 2015):

$$\begin{aligned}&\text{Slipping}: \quad \left|E\frac{\mathrm{d}\varepsilon_{0X}}{\mathrm{d}X}A\right| \geq F_f\\ &\text{Sticking}: \quad \left|E\frac{\mathrm{d}\varepsilon_{0X}}{\mathrm{d}X}A\right| < F_f\end{aligned} \tag{10}$$

where $F_f = (P_1 f_1 + P_2 f_2)b$ is the maximum friction force per unit length of helical wire. Note that the helical wire with a small θ always slips in advance because the smaller θ corresponds to the larger axial stress gradient during the sticking state (Kraincanic and Kebadze, 2001).

The above mentioned bending stiffness of the helical wire only considers the effect of the axial stress of the helical wires. Dong *et al*. (2013) investigated the effect of the local flexure of the helical wires on the bending stiffness. They found that the effect was negligible for the non-slipping state, but obvious for the full-slipping state. The contribution of the helical wire's local flexure to the bending stiffness can be described as follows:

$$\begin{aligned}EI_{bt} = \frac{1}{2}n\Big(&EI_Z\left(1+\sin^2\alpha\right)\cos\alpha + \\ &EI_Y\cos^7\alpha + GJ\sin^2\alpha\cos\alpha^5\Big)\end{aligned} \tag{11}$$

where n is the number of the helical wires on the tensile armor layer; and I_Y, I_Z, and J are the normal, transverse, and torsional moments of inertia, respectively.

The bending formulation of the cylindrical layer can be easily obtained. The related bending stiffness for the anti-wear layer can be calculated based on Eqs. (9) and (11). However, it may play a negligible role because of the small Young's modulus.

2.3 Stress at the critical point

The linearized Green–Lagrange strain at the critical point of the helical wire considering the local flexure can be expressed as follows (Skeie *et al*., 2012):

$$\begin{aligned}\varepsilon_X &= \varepsilon_{0X} - Y\Delta\kappa_Z + Z\Delta\kappa_Y\\ 2\varepsilon_{XY} &= Z\Delta\kappa_X\\ 2\varepsilon_{XZ} &= -Y\Delta\kappa_X\end{aligned} \tag{12}$$

where $\Delta\kappa_X$, $\Delta\kappa_Y$, and $\Delta\kappa_Z$ are the increments of the local twist, normal, and transverse curvatures around the Y and Z axes, respectively.

The local flexure increments induced by axisymmetric response are given as follows (Sævik, 2011):

$$\begin{aligned}\Delta\kappa_X &= \frac{u_z}{L}\frac{\sin^3(\alpha)\cos(\alpha)}{R} - \\ &\frac{u_r}{R}\frac{\sin^3(\alpha)\cos(\alpha)}{R} + \frac{\phi_z}{L}\cos^4(\alpha)\\ \Delta\kappa_Y &= -\frac{u_z}{L}\frac{\sin^2(\alpha)\cos^2(\alpha)}{R} + \frac{u_r}{R}\frac{\sin^2(\alpha)\cos^2(\alpha)}{R} + \\ &\frac{\phi_z}{L}\left(2\sin(\alpha)\cos^3(\alpha) + \sin^3(\alpha)\cos(\alpha)\right)\\ \Delta\kappa_Z &= 0\end{aligned} \tag{13}$$

This study presumes that the helical wire slips only along the axial direction (i.e., the loxodromic curve (Sævik, 2011)) and neglects the transverse slipping. Therefore, the increments of the local twist, normal, and transverse curvatures induced by the bending response are given as follows (Sævik, 2011; Skeie *et al*., 2012):

$$\begin{aligned}\Delta\kappa_X &= -\sin(\alpha)\cos^3(\alpha)\sin(\theta)\kappa\\ \Delta\kappa_Y &= \cos^4(\alpha)\sin(\theta)\kappa\\ \Delta\kappa_Z &= \cos(\alpha)\left(1+\sin^2(\alpha)\right)\cos(\theta)\kappa\end{aligned} \tag{14}$$

The von Mises equivalent stress is not only used in the ultimate strength analysis, but also often used in the multiaxial fatigue assessment (Benasciutti, 2014). Hence, it would also be analyzed in this study. The expression is written as follows:

$$\sigma_s = \sqrt{\left(E\varepsilon_x\right)^2 + 3\left(\left(G\varepsilon_{XY}\right)^2 + \left(G\varepsilon_{XZ}\right)^2\right)} \tag{15}$$

3 Validation

Witz (1996) reported an experimental study, where the tension–elongation and bending moment–curvature relationships were investigated in detail using a 2.5-inch unbonded flexible pipe. Table 1 shows the main parameters of this flexible pipe. Note that the experimental model did not include the outer sheath, instead of a fabric tape. This study employs this case to verify the above mentioned proposed axisymmetric and bending models. The friction coefficient between the metallic and anti-wear layers is 0.1 (Kraincanic and Kebadze, 2001).

Table 1 Main parameters of the unbonded flexible pipe

Layer No.	Inner diameter /mm	t/mm	α/(°)	E/MPa	ν
1	63.2	3.5	−87.5	2.05×10^5	0.29
2	70.3	4.9	/	284	0.30
3	80.1	6.2	−85.5	2.05×10^5	0.29
4	92.5	1.5	−84.2	301	0.30
5	95.5	3.0	−35.0	2.05×10^5	0.29
4	101.5	1.5	−84.7	301	0.3
5	104.5	3.0	35	2.05×10^5	0.29
Fabric tape	110.3	0.5	−84	600	0.3

Fig. 4 illustrates the axial force as a function of the elongation with the flexible pipe ends free to rotate. The present results are very similar with the mean value obtained using the models of different institutes (Witz, 1996). Compared with the experimental data, the present model overestimates the axial stiffness at a small elongation and fails to capture the unobvious hysteretic phenomenon, but predicts a relatively accurate axial stiffness with the increasing elongation. Fig. 5 shows the bending moment–curvature relationship under an internal pressure of 30 MPa. Before the bending analysis, the axisymmetric model is first applied to calculate the interlayer pressure. The numerically predicted hysteretic loop shows a good

agreement with the experimental data. Overall, the proposed model can reasonably model the axial and bending stiffness of the unbonded flexible riser.

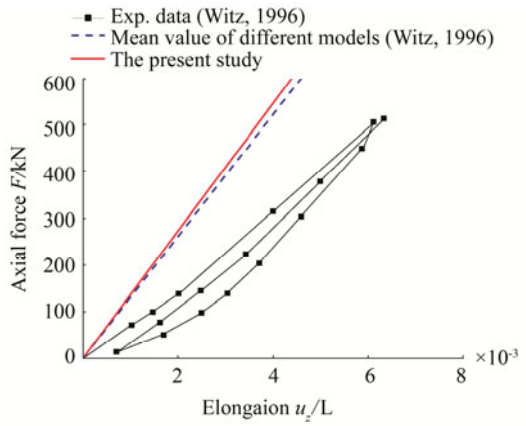

Fig. 4 Relationship between axial force and elongation

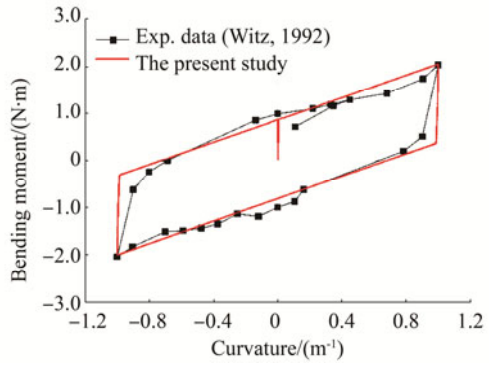

Fig. 5 Relationship between bending moment and curvature

4 Stress analysis of the helical wire

4.1 Stress at different angular positions

As regards the helical wire stress analysis, the predicted stress would remain constant when the slippage starts if only the axial stress is to be considered, and the stress induced by the local flexure is neglected. Moreover, a larger θ corresponds to a larger stress range according to Eq. (7). This condition may underestimate the stress range at critical positions and lead to a wrong selection of the fatigue failure position around the circumferential position. The present study takes the outer helical armor as an example and calculates the critical point stress at different angular positions by exerting a constant axial force and a regular curvature response on the above mentioned flexible pipe model: F=1.2×10^5 N, $\kappa\in$[−0.025 m^{-1}, 0.025 m^{-1}]. Fig. 6 demonstrates the stress variation with curvature. Considering the effect of the local flexure at a critical point, the stress still linearly increases with a low slope when the slippage starts, and the slope decreases with the increasing θ. Therefore, the fatigue failure position of the helical wire may be near a neutral surface when subjected to a large curvature variation (Hobbs and Ghavami, 1982; Sævik and Berge, 1995).

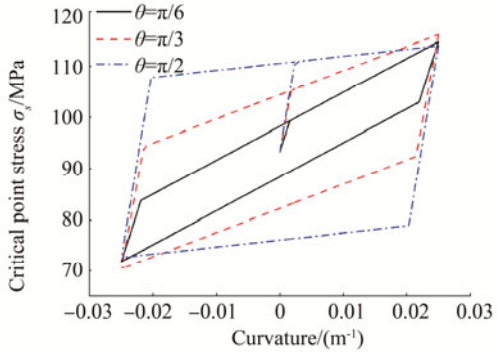

Fig. 6 Relationship between bending moment and curvature

4.2 Stress under an irregular curvature response

Published literatures mainly focused on the regular response analysis of flexible pipes and studied the full loop of the bending moment–curvature relationship based on the derived formula. The bending moment model in the present study calculates the axial stress of the helical wire around the circumferential position at each time step to judge whether slippage occurs, then obtains the bending stiffness for the next time step. Therefore, this model can be used in the irregular response analysis. An irregular curvature time history is exerted on the flexible pipe to demonstrate this feature (Fig. 7). For simplification, the irregular curvature response is directly obtained through the superposition of several sinusoidal responses, which ensures the slippage of the helical wire based on the critical curvature (Kraincanic and Kebadze, 2001). The axial force is F=1.2×10^5 N. The time increment of the calculation is set to 0.02 s. Fig. 8 illustrates the bending moment–curvature relationship, where point a is the bending initiation position. Regardless of the slippage occurrence or absence, the inverse route would follows the curve with a non-slipping bending stiffness until slippage occurs again, such as the inverse at points b and c. Fig. 9 shows the time history of the critical point stress. At the initial response marked by circle i, the stress $\theta=\pi/3$ exceeds that at $\theta=\pi/2$ because of the relative large stress increment with an increasing curvature when the helical wire slips. However, for the subsequent response, the larger θ corresponds to a larger stress because of the small curvature.

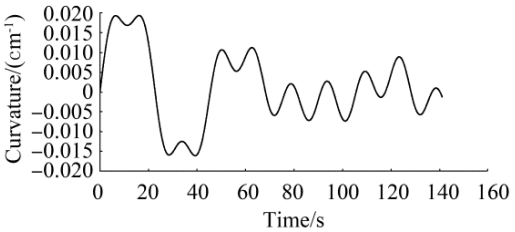

Fig. 7 Curvature time history

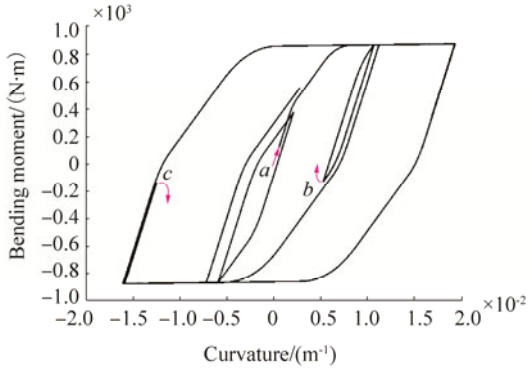

Fig. 8 Bending moment–curvature relationship under an irregular curvature load

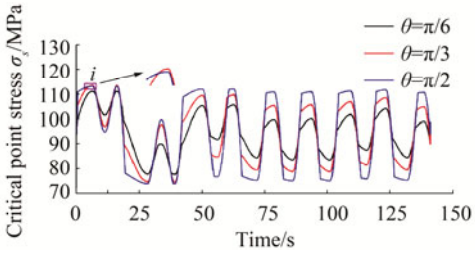

Fig. 9 Time histories of the critical point stresses at different angular points

4.3 Stress under an irregular bending moment

This section presents the response analysis of the flexible riser done by applying an irregular bending moment load and a constant axial force F=1.2×10^5 N. Fig. 10 shows the bending moment history. The bending moment during the initial time is not large enough to make the helical wire slip, thus the bending moment–curvature relationship follows the curve in region k (Fig. 11). Note that the quasi-static method is applied in this analysis.

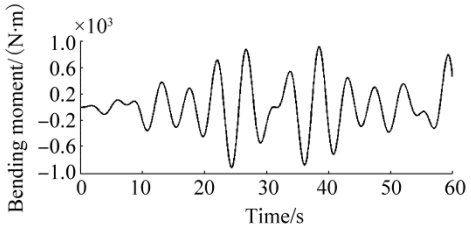

Fig. 10 Bending moment time history

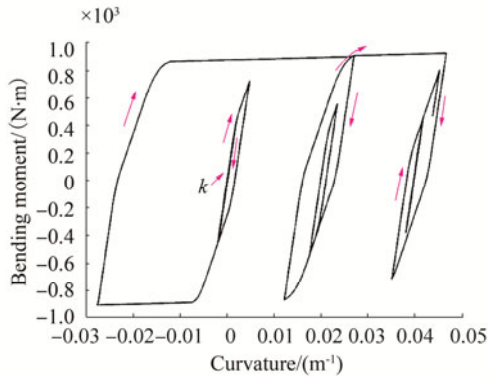

Fig. 11 Bending moment–curvature relationship under an irregular bending moment load

The conventional approach often assumes that the flexible riser is full-sticking or full-slipping in the global analysis. This study qualitatively discusses the effect of this approach on the predicted results. Fig. 12 shows a comparison of the curvatures predicted by three different models: 1) full-sticking, 2) full-slipping, and 3) present models. The curvature of the full-slipping model is very large because of the very small bending stiffness, and is divided by 100 in the plot. The full-sticking model has the same curvature with the present model during the initial time because the helical wire does not slip. However, the curvature of the present model significantly changes when the full-slipping occurs. The flexible riser maintains full-sticking from points a_1 to b_1, then partial-slipping from points b_1 to c_1 and full-slipping from points c_1 to d_1. Correspondingly, the critical point stress at θ = π/3 varies along $a_2 \rightarrow b_2 \rightarrow c_2 \rightarrow d_2$ in Fig. 13. Note that although the curvature changes relatively little from points a_1 to b_1, the corresponding critical point stress variation from points a_2 to b_2 is obvious because of the full-sticking. However, the large curvature variation from c_1 to d_1 results in a relatively small critical point stress variation from c_2 to d_2 because of the full-slipping. The increasing rate of the stress is small when slippage occurs, as discussed in Section 4.1.

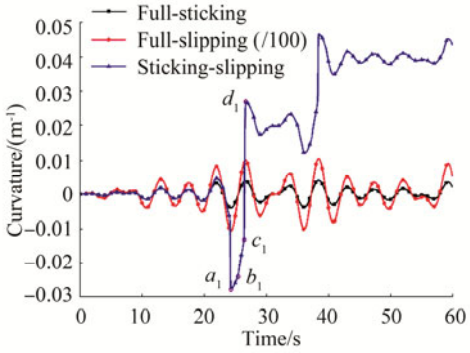

Fig. 12 Comparison of the curvature obtained from three different models

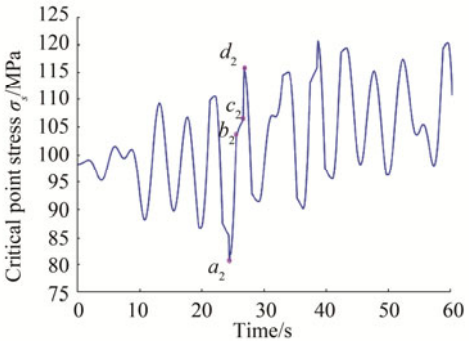

Fig. 13 Critical point stress at θ = π/3 under an irregular bending moment load

5 Conclusions

The present study proposed an analytical model for the flexible riser. The axisymmetric and bending analyzes for this model were performed separately by assuming that the

interlayer contact pressure remained constant during the bending response. Dummy springs, whose stiffness changed with the interlayer gap amplitude during the iterative calculation, were set between the layers to calculate the interlayer pressure under axisymmetric loads. The tangent stiffness matrix associated with the axisymmetric and the tangent bending stiffness were derived based on the virtual energy theory. The axial stress gradients of the helical wire around the circumferential direction were calculated at each time step in the bending analysis to judge whether slippage occurs. The slipping region was then obtained to determine the bending stiffness for the next time step.

This model was feasible for an irregular bending response. The proposed model was verified against an experimental model in the literature. The predicted axial force–elongation and bending moment–curvature relationships showed good agreement with the experimental data.

The bending moment–curvature relationship under an irregular response was demonstrated based on the proposed model. The critical point stress of the helical wire was also investigated by considering the local flexure. The results indicated that the critical point stress still linearly increased with the increasing curvature after slipping, but the slope was smaller than that before slipping. This result was different from that of the traditional approach, which only considered the axial stress that would remain constant after slipping. In addition, the larger angular position θ corresponded to a larger slope after slipping, which was in contrast with the law before slipping. Therefore, a small angular position θ may have a relatively large critical point stress under a large curvature. The flexible riser responses obtained from the conventional models with a constant bending stiffness and those from the present model were also compared. The curvature predicted by the present model sharply increased when slippage occurred and was obviously larger than that predicted by the full-sticking model.

In conclusion, the proposed model can well capture the hysteretic relationship between the bending moment and the curvature. It can also predict the helical wire stress at a critical point under an irregular response. Therefore, this model can be implemented in an unbonded flexible riser global analysis for a more accurate fatigue damage prediction.

Appendix

$$K_{11}=\sum_{i=1}^{N} g_{11,i}$$

$$g_{11,i}=\begin{cases}\dfrac{(E_1A)_i}{1-(v_{12}v_{21})_i} & \text{Cylinderical layer}\\ n_iE_iA_i\cos^3(\alpha_i) & \text{Helical armor}\end{cases} \tag{A1}$$

$$K_{12}=\sum_{i=1}^{N} g_{12,i}$$

$$g_{12,i}=\begin{cases}0 & \text{Cylinderical layer}\\ n_iE_iA_iR_i\sin(\alpha_i)\cos^2(\alpha_i) & \text{Helical armor}\end{cases} \tag{A2}$$

$$K_{1j}=\begin{cases}\dfrac{(v_{12}E_1A)_i}{1-(v_{12}v_{21})_i} & \text{Cylinderical layer}\\ n_iE_iA_i\cos(\alpha_i)\sin^2(\alpha_i) & \text{Helical armor}\end{cases} \tag{A3}$$

$(j>2;\ i=j-2)$

$$K_{22}=\sum_{i=1}^{N} g_{22,i}$$

$$g_{22,i}=\begin{cases}(G_{12}I_z)_i & \text{Cylinderical layer}\\ n_iE_iA_iR_i^2\sin^2(\alpha)\cos(\alpha_i) & \text{Helical armor}\end{cases} \tag{A4}$$

$$K_{2j}=\begin{cases}0 & \text{Cylinderical layer}\\ n_iE_iA_iR_i\sin^3(\alpha_i) & \text{Helical armor}\end{cases} \tag{A5}$$

$(j>2 \text{ and } i=j-2)$

$$K_{jj}=g_{jj}+h_{jj}$$

$$g_{jj}=\begin{cases}\dfrac{(EA)_i}{1-(v_{12}v_{21})_i} & \text{Cylinderical layer}\\ n_iE_iA_i\dfrac{\sin^4(\alpha_i)}{\cos(\alpha_i)} & \text{Helical armor}\end{cases}$$

$$h_{jj}=\begin{cases}\dfrac{1}{2}k_iR_i^2 & i=1\\ \dfrac{1}{2}k_{i-1}R_{i-1}^2 & i=N\\ \dfrac{1}{2}\left(k_{i-1}R_{i-1}^2+k_iR_i^2\right) & 1<i<N\end{cases} \tag{A6}$$

$(j>2 \text{ and } i=j-2)$

$$K_{j(j+1)}=-\frac{1}{2}k_iR_iR_{i+1} \quad 2<j<2+N \text{ and } i=j-2 \tag{A7}$$

$$\bar{F}=F+\pi\left(P_{\text{in}}R_2^2-P_{\text{out}}R_N^2\right) \tag{A8}$$

$$\bar{P}_{j-2}=\begin{cases}2\pi P_{\text{in}}R_2^2 & j-2=2\\ -2\pi P_{\text{out}}R_N^2 & j-2=N\\ 0 & j-2\neq 2 \text{ and } \neq N\end{cases} \tag{A9}$$

where A is the layer cross-section area for the cylindrical layer or wire cross-section area for the helical armor.

References

Bahtui A, Bahai H, Alfano G, 2009. Numerical and analytical modeling of unbonded flexible risers. *Journal of Offshore Mechanics and Arctic Engineering*, **131**(2), 021401. DOI: 10.1115/1.3058700

Benasciutti D, 2014. Some analytical expressions to measure the accuracy of the equivalent von Mises stress in vibration multiaxial fatigue. *Journal of Sound and Vibration*, **333**(18), 4326-4340. DOI: 10.1016/j.jsv.2014.04.047

De Sousa JRM, Campello GC, Kwietniewski CEF, 2014. Structural response of a flexible pipe with damaged tensile armor wires under pure tension. *Marine Structures*, **39**, 1-38. DOI: 10.1016/j.marstruc.2014.06.002

De Sousa JRM, De Sousa FJM, De Siqueira MQ, 2012. A theoretical approach to predict the fatigue life of flexible pipes. *Journal of Applied Mathemathics*, **2012**(6), 1927-1936. DOI: 10.1155/2012/983819

de Sousa JRM, Magluta C, Roitman N, 2009. On the response of flexible risers to loads imposed by hydraulic collars. *Applied Ocean Research*, **31**(3), 157-170.
DOI: 10.1016/j.apor.2009.07.005

Dong LL, Huang Y, Zhang Q, 2013. An analytical model to predict the bending behavior of unbonded flexible pipes. *Journal of Ship Research*, **57**(3), 171-177.
DOI: 10.5957/JOSR.57.3.120023

Dong LL, Tu SS, Huang Y, Dong GH, Zhang Q, 2015. A model for the biaxial dynamic bending of unbonded flexible pipes. *Marine Structures*, **43**, 125-137.
DOI: 10.1016/j.marstruc.2015.07.001

Hobbs RE, Ghavami K, 1982. The fatigue of structural wire strands. *International Journal of Fatigue*, **4**(2), 69-72.
DOI: 10.1016/0142-1123(82)90062-7

Kraincanic I, Kebadze E, 2001. Slip initiation and progression in helical armoring layers of unbonded flexible pipes and its effect on pipe bending behavior. *Journal of Strain Analysis for Engineering Design*, **36**(3), 365-275.
DOI: 10.1243/0309324011514458

Lanteigne J, 1985. Theoretical estimation of the response of helically armored cables to tension, torsion, and bending. *Journal of Applied Mechanics*, **52**(2), 423-432.
DOI: 10.1115/1.3169064

Leroy JM, Estrier P, 2001. Calculation of stresses and slips in helical layers of dynamically bent flexible pipes. *Oil and Gas Science and Technology*, **56**(6), 545-554.
DOI: 10.2516/ogst:2001044

McNamara JF, Harte AM, 1989. Three dimensional analytical simulation of flexible pipe wall structure. *Journal of Offshore Mechanics and Arctic Engineering*, **114**(2), 69-75.
DOI: 10.1115/1.2919961

Sævik S, 2011. Theoretical and experimental studies of stresses in flexible pipes. *Computers and Structures*, **89**(23-24), 2273-2291.
DOI: 10.1016/j.compstruc.2011.08.008

Sævik S, Berge S, 1995. Fatigue testing and theoretical studies of two 4 inch flexible pipes. *Engineering Structures*, **17**(4), 276-292.
DOI: 10.1016/0141-0296(95)00026-4

Skeie G, Sødahl N, Steinkjer O, 2012. Efficient fatigue analysis of helix elements in umbilicals and flexible risers: Theory and applications. *Journal of Applied Mathematics*, **2012**(1), 246812.
DOI: 10.1155/2012/246812

Tan ZM, Quiggin P, Sheldrake T, 2007. Time domain simulation of the 3D bending hysteresis behavior of an unbonded flexible riser, *Journal of Offshore Mechanics and Arctic Engineering*, **131**(3), 307-314.
DOI: 10.1115/1.3058698

Tang MG, Yang C, Yan J, Yue QJ, 2015. Validity and limitation of analytical models for the bending stress of a helical wire in unbonded flexible pipes. *Applied Ocean Research*, **50**, 58-68.
DOI: 10.1016/j.apor.2014.12.004

Wang W, Chen G, 2011. Analytical and numerical modeling for flexible pipes. *China Ocean Engineering*, **25**(4), 737-746.
DOI: 10.1007/s13344-011-0059-9

Witz JA, 1996. A case study in the cross-section analysis of flexible risers. *Marine Structures*, **9**(9), 885-904.
DOI: 10.1016/0951-8339(95)00035-6

Witz JA, Tan Z, 1992a. On the axial-torsional structural behavior of flexible pipe, umbilicals and marine cables. *Marine Structures*, **5**(2), 205-227.
DOI: 10.1016/0951-8339(92)90029-O

Witz JA, Tan Z, 1992b. On the flexural structural behaviour of flexible pipes, umbilicals and marine cables. *Marine Structures*, **5**(2-3), 229-249.
DOI: 10.1016/0951-8339(92)90030-S